

THE INITIAL MASS FUNCTION OF THE STELLAR ASSOCIATION NGC 602 IN THE SMALL MAGELLANIC CLOUD WITH HUBBLE SPACE TELESCOPE ACS OBSERVATIONS¹

MARKUS SCHMALZL, DIMITRIOS A. GOULIERMIS

Max-Planck-Institute for Astronomy, Königstuhl 17, 69117 Heidelberg, Germany;
schmalzl@mpia.de, dgoulier@mpia.de

ANDREW E. DOLPHIN

Raytheon Corporation, 870 Winter Street Waltham, MA 02451, USA; adolphin@raytheon.com

AND

THOMAS HENNING

Max-Planck-Institute for Astronomy, Königstuhl 17, 69117 Heidelberg, Germany; henning@mpia.de

Accepted for Publication in ApJ

ABSTRACT

We present our photometric study of the stellar association NGC 602 in the wing of the Small Magellanic Cloud (SMC). The data were taken in the filters $F555W$ and $F814W$ using the *Advanced Camera for Surveys* (ACS) on-board the *Hubble* Space Telescope (HST). Photometry was performed using the ACS module of the stellar photometry package DOLPHOT. We detected more than 5,500 stars with a magnitude range of $14 \lesssim m_{555} \lesssim 28$ mag. Three prominent stellar concentrations are identified with star counts in the observed field, the association NGC 602 itself, and two clusters, one of them not being currently in any known catalog. The Color-Magnitude Diagrams (CMDs) of both clusters show features typical for young open clusters, while that of the association reveals bright main sequence (MS) and faint pre-main sequence (PMS) stars as the members of the system. We construct the initial mass spectrum (IMS) of the association by applying an age-independent method of counting the PMS stars within evolutionary tracks, while for the bright MS stars we transform their magnitudes to masses with the use of mass-luminosity relations. The IMS of NGC 602 is found to be well represented by a single-power law, corresponding to an Initial Mass Function (IMF) of slope $\Gamma \approx -1.2$ for $1 \lesssim M/M_{\odot} \lesssim 45$. This indicates that the shape of the IMF of a star forming system in the SMC for stars with masses higher than $1 M_{\odot}$ seems to be quite similar to the field IMF in the solar neighborhood.

Subject headings: galaxies: star clusters — Magellanic Clouds — open clusters: individual(NGC 602) — stars: evolution — stars: pre-main-sequence stars: luminosity function, mass function

1. INTRODUCTION

The Small Magellanic Cloud (SMC), the second closest undisrupted neighboring dwarf galaxy to our own (after the Large Magellanic Cloud; LMC) is an ideal laboratory to investigate star formation at an environment similar to the early universe. Its metallicity is by a factor of 5 lower than the solar metallicity (Luck et al. 1998; Ven 1999), and its dust-to-gas ratio is measured to be up to 10 times lower than in the Milky Way (e.g. Stanimirovic et al. 2000). Therefore, the SMC may be considered as an excellent local template for studying primordial star formation, providing insight into the processes at work in the early universe. The recent star formation process in the SMC is characterized by a rich sample of H II regions (Henize 1956; Davies et al. 1976) linked to young stellar systems, the *stellar associations*, known for their early-type stellar content and loose structure (e.g. Kontizas et al. 1999). The small distance of the SMC from us (≈ 60 kpc) allows us to resolve from space individual stars down to $M_V \approx 10$ mag, and consequently the study of its low-mass young stellar content and the corresponding Initial Mass Function (IMF) becomes unusually accessible.

Stellar associations contain the richest sample of young bright stars in a galaxy. Our knowledge on the young massive stars of the Magellanic Clouds (MCs) has been collected

from ground-based studies of young stellar associations (see e.g. Massey 2006 and references therein). However, our knowledge of the low-mass stellar membership and the corresponding IMF in star-forming regions of the MCs is quite incomplete. A first attempt to define the low-mass population of a stellar association in the MCs was made by Gouliermis et al. (2005). In their photometric study of the LMC association LH 52 with data from the *Wide-Field Planetary Camera 2* (WFPC2), these authors test the hypothesis that sub-solar-mass stars *can be* detected in the MCs. They found that all faint main sequence stars, which are observed in the area of the association, belong to the general field of the LMC and not to the system. The field-subtracted mass function of LH 52, which accounts for its IMF was found by these authors with a slope $\Gamma \sim -1.1$ for main sequence stars down to $M \approx 1 M_{\odot}$. This slope is comparable, but somewhat more shallow than a typical Salpeter (1955; $\Gamma \sim -1.35$) IMF. An IMF well reproduced by a power law with a slope consistent with Salpeter's was also found by Sirianni et al. (2002) in the central regions (within $30''$) of the young SMC star cluster NGC 330.

The investigation by Gouliermis et al. (2005) revealed, for the first time, that the low-mass stellar content of stellar associations in the MCs is still in its pre-main sequence (PMS) phase, as is the case of nearby galactic associations (Briceño et al. 2007). Gouliermis et al. (2006a) discovered in LH 52 about 500 low-mass PMS stars down to $\sim 0.5 M_{\odot}$, easily distinguishable in the $m_{555} - m_{814}$, m_{555} Color-Magnitude

¹ Research supported by the Deutsche Forschungsgemeinschaft (German Research Foundation)

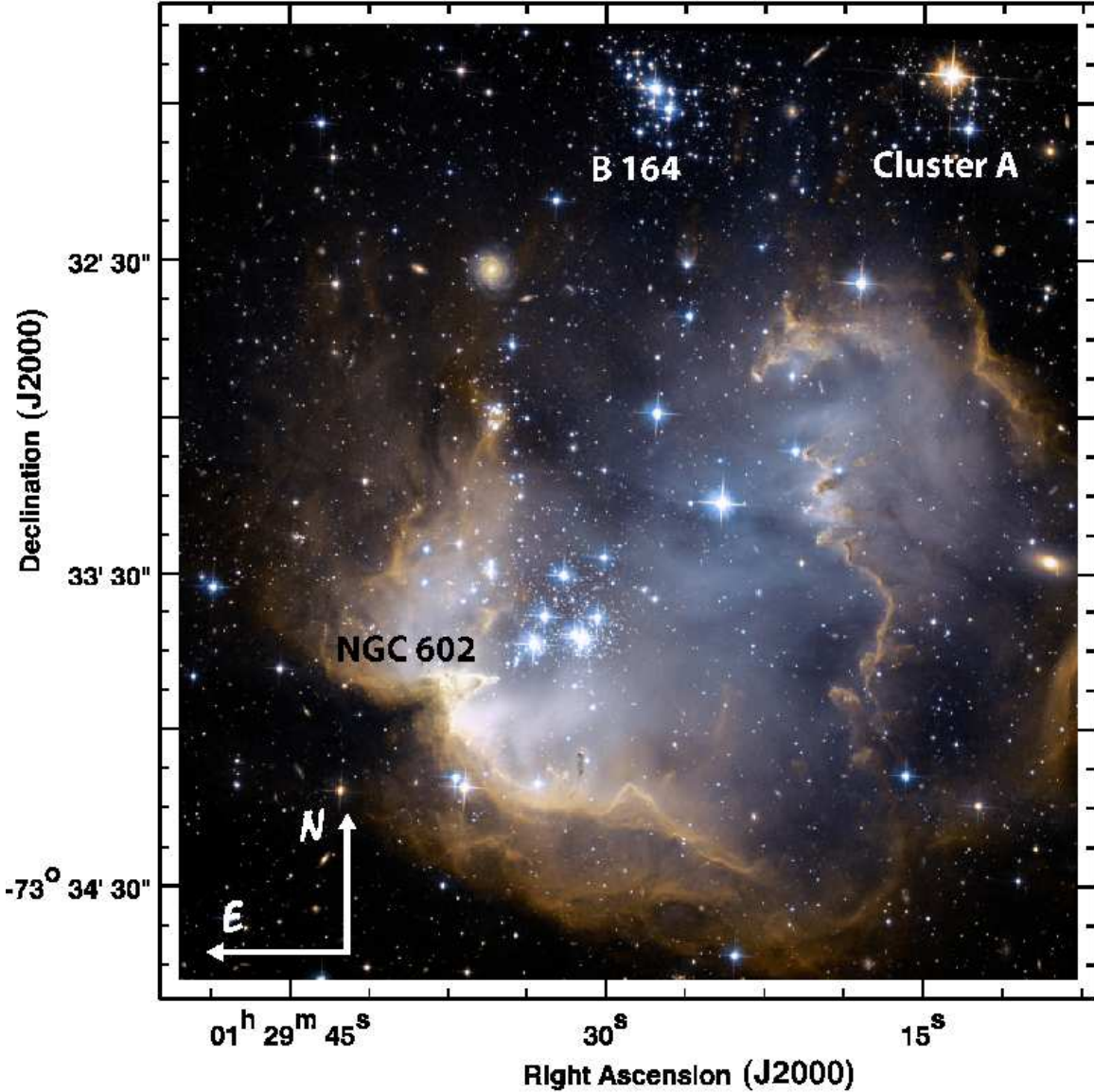


FIG. 1.— Color-composite image of the field around NGC 602, constructed from observations with HST/ACS in the filters $F555W$, $F814W$ and $F658N$. The association itself lies at the center of the field, located almost in the middle of the shell-like emission nebula N 90. Directly north of the association lies the open cluster B 164 (Bruck 1976), and the newly discovered “cluster A” covers the north-western edge of the field. All three systems are confirmed as statistically significant stellar concentrations from star counts shown in Figure 4. Credit: NASA, ESA, and the Hubble Heritage Team (STScI/AURA)-ESA/Hubble Collaboration.

TABLE 1
LOG OF THE OBSERVATIONS

Visit	RA	DEC	T_{expo}	
			F555W	F814W
Dataset	(J2000.0)			
J92F05	01 29 28.21	-73 33 16.7	430	453
	01 29 28.52	-73 33 16.4	430	453
	01 29 27.89	-73 33 16.9	430	453
	01 29 27.57	-73 33 17.1	430	453
	01 29 27.57	-73 33 17.1	3	2
	01 29 27.25	-73 33 17.4	430	453
J92FA6	01 29 27.57	-73 33 17.1	3	2

NOTE. — Datasets refer to HST archive catalog. Exposure times (T_{expo}) per filter are given in seconds. Units of right ascension are hours, minutes, and seconds, and units of declination are degrees, arcminutes, and arcseconds.

Diagram (CMD), extending the sub-solar stellar membership of MCs stellar associations to their PMS populations. Naturally, these stars should be considered as the best tracers of the sub-solar IMF in the MCs, but the WFPC2 data, being limited by completeness, allowed the construction of the PMS IMF of LH 52 only for the mass range $0.8 - 1.4 M_{\odot}$. This IMF was found to correspond to a power-law with a slope of $\Gamma \sim -1.26$. Previous PMS studies in the MCs focus on the surrounding field of supernova 1987A (e.g. Panagia et al. 2000), where the sample is limited, and the star-burst of 30 Doradus (e.g. Zinnecker 1998; Sirianni et al. 2000; Brandner et al. 2001), where crowding and high extinction limit the detection of stars to $1 - 2 M_{\odot}$ (Romaniello et al. 2006).

Over the last years, stellar associations in the SMC gained increasing scientific interest, as the investigation of their bright OB stars was complimented by new studies on their PMS stars (e.g. Nota et al. 2006; Gouliermis et al. 2006b; Sabbi et al. 2007; Hennekemper et al. 2008). These studies

TABLE 2

SAMPLE FROM THE PHOTOMETRIC CATALOG OF STARS FOUND IN THIS STUDY IN THE REGION OF NGC 602/N 90 WITH HST/ACS IMAGING

#	R.A. (J2000.0)	DECL. (J2000.0)	m_{555} (mag)	σ_{555} (mag)	m_{814} (mag)	σ_{814} (mag)
1	01 29 54.828	-73 32 31.524	14.690	0.004	13.217	0.003
2	01 29 24.581	-73 33 16.236	13.881	0.002	14.128	0.003
3	01 29 14.220	-73 31 53.256	14.717	0.003	13.354	0.002
4	01 29 33.310	-73 33 44.496	14.270	0.002	14.508	0.004
5	01 29 31.051	-73 33 43.056	15.371	0.004	15.612	0.007
6	01 29 28.301	-73 31 57.432	15.341	0.004	15.288	0.006
7	01 29 36.485	-73 34 12.108	16.412	0.007	14.993	0.005
8	01 29 32.837	-73 33 39.024	15.467	0.004	15.673	0.007
9	01 29 31.992	-73 33 30.924	15.594	0.005	15.796	0.007
10	01 29 27.768	-73 32 59.496	15.730	0.005	15.699	0.007
11	01 29 18.286	-73 32 33.468	16.052	0.006	15.322	0.006
12	01 29 31.094	-73 33 43.272	15.816	0.005	16.074	0.008
13	01 29 31.411	-73 33 42.336	15.663	0.005	15.871	0.008
14	01 29 14.249	-73 31 53.220	17.910	0.020	16.655	0.018
15	01 29 32.942	-73 34 10.956	16.232	0.006	16.377	0.010

NOTE. — Magnitudes are given in the Vega system. Units of right ascension are hours, minutes, and seconds, and units of declination are degrees, arcminutes, and arcseconds. Table 2 is available in its entirety in the electronic edition of the *Astrophysical Journal*. A portion is shown here for guidance regarding its form and content.

TABLE 3
POPULATIONS SUMMARY IN THE IDENTIFIED STELLAR SYSTEMS

Name	n_{stars}	ρ (pc $^{-2}$)	f_{PMS}	f_{UMS}	f_{LMS}
NGC 602	855	5.6	0.86	0.07	0.04
B 164	356	2.9	0.03	0.27	0.62
Cluster A	171	2.0	0.05	0.21	0.63
Field	230	1.1	0.16	0.08	0.66

NOTE. — The total stellar numbers of the systems, n_{stars} , are field-subtracted (see § 4.3.1), and refer to the area of each system defined with star counts. The total number of field stars, shown in the last row, refers to the area defined as the best representative of the field due to its emptiness. The fractions f give the number of one stellar species over the total stellar numbers in every area. The most significant numbers are highlighted. It is interesting to note that both B 164 and Cluster A have almost identical numbers of UMS and LMS stars, and that their LMS fractions are comparable to that of the field.

were facilitated by the unique combination of high-resolving power with a wide field-of-view provided by the *Advanced Camera for Surveys* (ACS) on-board *HST*. In the present study we deal with the IMF of the young stellar association NGC 602, related to the bright H II region LHA 115-N90, or in short N 90 (Henize 1956). The region NGC 602/N 90, being located in the wing of the SMC, has the advantage of avoiding the densest parts of the galaxy. As a consequence, the confusion of its stellar content with that of the general SMC field, which extends in a wide depth along the line-of-sight, is rather low. McCumber et al. (2005) found in their investigation on field stars in the SMC wing that after a long period of constant star formation, there was a burst in activity within the last 1 Gyr. The lack of γ -ray, X-ray or far-UV sources in the region of NGC 602/N 90 suggests that this excess in the star formation of the area was possibly triggered by encounters with the LMC and/or the Milky Way. Most likely, all major star-forming events in the SMC are initiated by these tidal interactions. In the first part of our investigation of the region NGC 602/N 90 (Gouliermis et al. 2007) we present the results of our photometric study from obser-

vations with the *Infrared Array Camera* (IRAC) on-board the *Spitzer Space Telescope*. We report the detection of 22 candidate Young Stellar Objects (YSOs), which are located at the edge of N 90, suggesting that they are the products of star formation triggered by the central association NGC 602.

The recent release of the HST/ACS observations of the region of NGC 602/N 90 offers a unique opportunity for the comprehensive photometric analysis of both its bright and faint stellar content, and the construction of the complete IMF throughout the whole observed mass range. Our photometry, which reaches the limit of $m_{555} \gtrsim 26.5$ mag, providing one of the most complete stellar samples ever collected for star-forming regions in the SMC, is described in § 2. We investigate the morphology of the observed region and the spatial distribution of the detected stars in § 3, and in § 4 we discuss the nature of the detected stellar species and present the CMDs of the three major stellar concentrations in the observed field. In § 4 we also present the subtraction of the contribution of the field from the observed CMDs, and we estimate the reddening towards the identified systems. A detailed description of the stellar members of the association NGC 602 is also given in § 4. The Luminosity Functions of the identified stellar systems are constructed in § 5. In § 6 a comprehensive construction of the IMF of NGC 602, as well as of the two additional star clusters in the region is presented. Conclusions are given in § 7.

2. OBSERVATIONS AND PHOTOMETRY

The data used in our analysis are obtained with the Wide Field Channel (WFC) of the ACS within the *HST* GO Program 10248 on July 14 (Dataset: J92F05) and July 18 (Dataset: J92FA6) 2004. Images are taken in the $F555W$ and $F814W$ filters. A single ACS/WFC pointing covering $\approx 3'.4 \times 3'.4$ was centered on NGC 602/N 90. At the distance of the SMC this field-of-view (FoV) corresponds to an extent of $\approx 57 \times 57$ pc. The first visit (J92F05) includes five long exposures taken with a dithering pattern in order to cover the inter-chip gap of the camera and one short exposure with a single pointing to cope with the saturation of the brightest stars. Within the second visit (J92FA6) a short exposure was also taken in order to remove cosmic rays that were unintentionally included during the first visit. In Table 1 we give a summary of the different data sets used in this investigation. A color-composite image of the observed field is shown in Fig. 1.

Photometry was performed with the ACS module of the package DOLPHOT² (Ver. 1.0), especially designed for ACS. We followed the photometric process, as it is described by Gouliermis et al. (2006b). The pipeline-reduced FITS files were obtained from the *HST* Data Archive. We used the package *multidrizzle* (Koekemoer et al. 2002) following the ACS data handbook to clean the images of residual warm pixels and cosmic rays and to construct a deep reference drizzled image to be used for the photometry. All exposures were photometered simultaneously, using the $F814W$ drizzled frame as the position reference. Photometric calibrations and transformations were made according to Sirianni et al. (2005). Charge Transfer Efficiency corrections were applied according to ACS ISR 04-06. We cleaned our photometric catalog from bad detections using DOLPHOT's star quality parameters, as described also by Gouliermis et al. (2006b). The final

² The ACS module of DOLPHOT is an adaptation of the photometry package HSTphot (Dolphin 2000). It can be downloaded from <http://purcell.as.arizona.edu/dolphot/>.

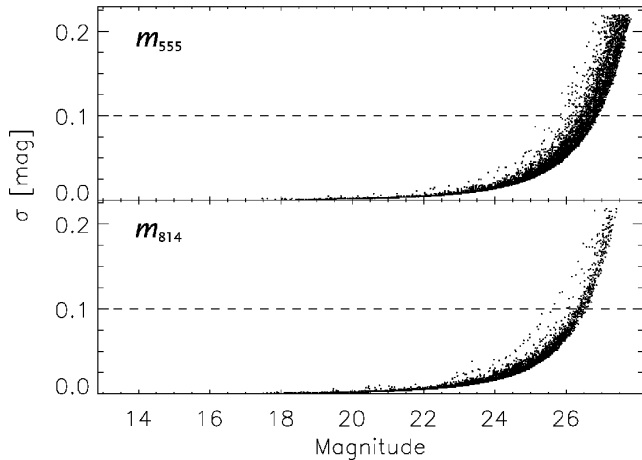


FIG. 2.— Typical photometric uncertainties in both m_{555} and m_{814} bands as derived by DOLPHOT from all data sets.

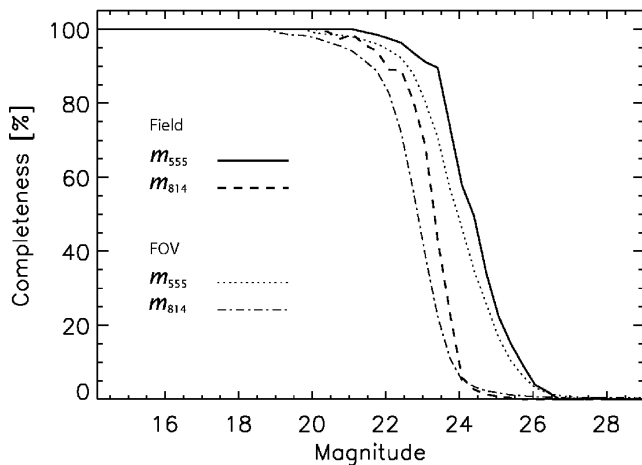


FIG. 3.— Completeness for all stars in the observed FoV and in the area selected as the most representative of the local field the SMC. The field being less contaminated by the nebula and less crowded than the association NGC 602 exhibits a higher completeness than the overall FoV.

photometric catalog includes 5,626 stars in total detected in both filters. The full length of this catalog with the RA, DEC coordinates (in J2000) and their magnitudes in each filter (in the Vega system) of these stars is available in electronic form in Table 2. Astrometric solutions for the detected stars are derived from the $F814W$ drizzled frame with the use of the application *xy2sky* of the WCSTools package³.

Typical uncertainties of our photometry as a function of the magnitude for both filters are given in Fig. 2. The completeness of the data was evaluated by artificial star experiments with the use of lists of almost 400,000 artificial stars created with the utility *acsfakelist* of DOLPHOT. The completeness is found to be spatially variable, depending on the crowding of each region. This is shown in Fig. 3, where the completeness factors for the whole observed field, as well as of the area selected as the most representative of the background field, due to its emptiness, are plotted for both filters. The area, which from here on we refer to as simply the “field”, is selected as the most *empty area* of the western part of the observed FoV. This selection was based on our recent results from *Spitzer*/IRAC, which show that this part of NGC 602/N 90 is the less contaminated by dust emission

³ The WCSTools package is available at CfA at <http://tdc-www.harvard.edu/software/wcstools/>.

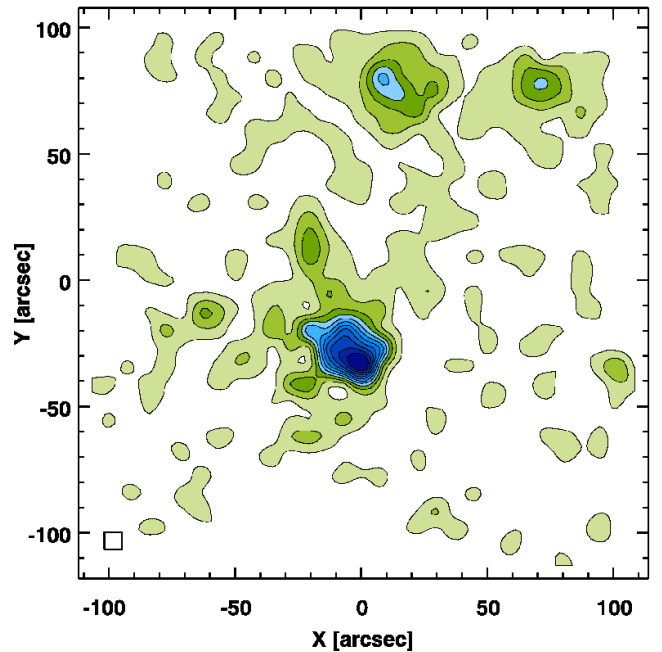


FIG. 4.— Isodensity contour map for all stars with photometric errors $\sigma_V \leq 0.1$ mag using grid elements of size $7''$, shown as the small box at the bottom-left corner of the map. The first isopleth corresponds to the mean background density. The next isopleths are plotted in steps of the standard deviation σ . The bluish contours correspond to stellar density equal or higher than the 3σ level. All three stellar systems in the region are revealed as significant stellar concentrations.

(Gouliermis et al. 2007).

3. MORPHOLOGY OF THE REGION OF NGC 602/N 90

The prominent bright stellar concentration almost at the center of the observed ACS/WFC field, shown in Fig. 1, is the association NGC 602. The bright emission nebula, N 90, can also be seen in the image, because of the $H\alpha$ emission, included in the $F658N$ filter (centered at 658.4 nm). A small contribution from [NII] is also included in this filter. The association is surrounded by a ring-like feature highlighted by the gas emission, and ribbon-like structures pointing towards the center can be seen to the southeastern and northwestern of the ring. These structures have been identified by Gouliermis et al. (2007) as the SMC analogs of the “Pillars of creation” originally detected in the Galactic H II region M 16 (Hester et al. 1996). They clearly indicate ongoing star formation on the rim of the ring-like structure, probably driven by the stellar winds and UV radiation of the brightest stars in NGC 602.

The stellar association is not the only stellar concentration inside the observed FoV. North of the association lies the open cluster B 164 (Bruck 1976) which is also known as NGC 602b (Westerlund 1964). Next to B 164 and to the west lies a third stellar concentration. It shows to be a cluster, which does not belong to any catalog of known objects in this region. From here on we refer to this cluster as “Cluster A”. All three stellar systems are easily revealed by the spatial distribution of all stars detected with our photometry in the region, as discussed in the next section.

3.1. Spatial Distribution of the Stars in NGC 602/N 90

In order to reveal the spatial distribution of the detected stars and the morphology of any stellar concentrations in the observed region, we performed star counts on our photometric catalog (a sample of this catalog is shown in Table 2). Stars with photometric uncertainties $\sigma_V \geq 0.1$ mag were not con-

sidered. The constructed isodensity contour map is shown in Fig. 4. The coordinate system used for this map, as well as the ones shown later is the Cartesian (X, Y) system of the pixel coordinates of WFC, transformed to seconds of arc, in respect to the central pixel of the FoV.

Star counts were performed in a quadrilateral grid divided in elements with sizes 140×140 WFC pix^2 each, which correspond to $7'' \times 7''$ (or $\approx 2 \text{ pc} \times 2 \text{ pc}$ at the distance of the SMC). This size was selected as the optimum to map any fine structure, which might exist within the clusters. The selection of larger size for the grid elements would reveal a smoother version of the map of Fig. 4. The first isopleth in the contour map indicates the mean background density, whereas the subsequent levels are drawn in steps of 1σ , where σ is the standard deviation of the background density. All contours with density equal or higher than the 3σ level, which is chosen as the density threshold of the statistically significant stellar concentrations are drawn with bluish colors. All three star clusters in the region are revealed in this map with NGC 602 being the dominant stellar system, seen almost at its center. The density peaks for both B 164 and Cluster A do exceed the 3σ limit as well. Smaller compact density peaks can be seen in the map below the 3σ limit. They are typical density fluctuations, due to the small size selected for the grid elements.

4. STELLAR POPULATIONS IN THE REGION OF NGC 602/N 90

4.1. Color-Magnitude Diagram

The $m_{555} - m_{814}$, m_{555} color-magnitude diagram (CMD) of all stars in our photometric catalog is shown in Fig. 5, which indicates that our photometry provides accurate magnitudes (with $\sigma_{555} \lesssim 0.1 \text{ mag}$) for stars with $m_{555} \lesssim 26.5 \text{ mag}$. Different groups of stellar types can easily be distinguished in this CMD. There is a prominent well populated main sequence (MS), which extends from the detection limit up to $m_{555} \approx 14 \text{ mag}$, and a rich population of pre-main sequence (PMS) stars located on the red part of the MS. We select regions of the CMD, each covering different types of stars. The tentative limits of these regions are also shown in Fig. 5. We split the MS into its upper (brighter) and lower (fainter) parts (UMS and LMS respectively). According to the ZAMS isochrone from the model grid designed by Girardi et al. (2002) for the ACS filter system, the limit between UMS and LMS stars of $m_{555} = 22.6 \text{ mag}$ corresponds to a stellar mass of $M \approx 1.2 M_{\odot}$.

The brighter limit of the PMS region in the CMD is being chosen around $m_{555} \approx 22.3 \text{ mag}$. Probably, a brighter limit would allow us to include the brighter PMS stars and the transition region between PMS and MS (turn-on), but this part of the CMD is contaminated by the old stellar population of the field of the galaxy (e.g. McCumber et al. 2005), as seen by its loose red giant branch (RGB). The low numbers of widely scattered stars in the RGB part of the CMD and the absence of any clearly detectable turn-off indicates that only a small fraction of the evolved field stars can be seen in the observed region, probably due to extinction by the dust. Indeed, *Spitzer*/IRAC observations of NGC 602/N 90 have shown in the $8 \mu\text{m}$ band strong dust emission from the area, which surrounds the central ‘‘hole’’ in the H II region, where NGC 602 is located (Gouliermis et al. 2007).

4.2. Stellar Populations in the Systems of the Region

Isodensity contour maps from counts of the three most important stellar types in the CMD of Fig. 5 exhibit a strong

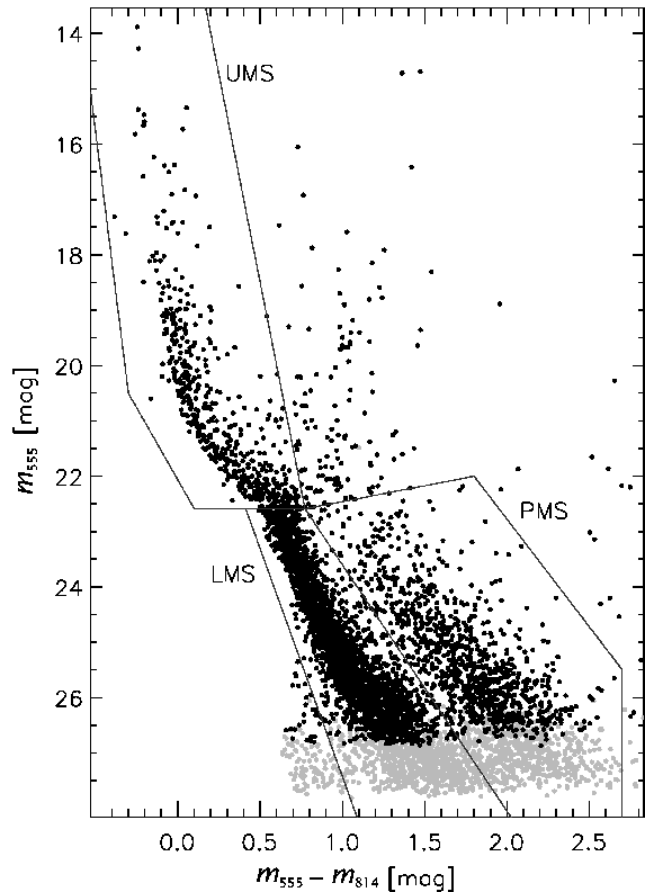


FIG. 5.— The $m_{555} - m_{814}$, m_{555} CMD of all stars detected in the region of NGC 602/N 90. Stars with photometric uncertainties larger than 0.1 mag (Fig. 2) are shown as grey dots. The drawn lines indicate the tentative limits, which separate the different stellar species included in the catalog of detected stars: The Upper Main Sequence (UMS), the Lower Main Sequence (LMS), and the Pre-Main Sequence (PMS) stars.

spatial distinction between UMS, LMS and PMS stars. This is shown in the bottom panels of Fig. 6 (Figs. 6a, 6b, 6d and 6e). The contour maps of this figure are constructed with the same method as the map of Fig. 4 (see § 3.1), and the lowest density isopleth shown corresponds to 3σ above the local background density. These maps reveal again all three important stellar systems in the region (NGC 602, B 164 and Cluster A), but they demonstrate that these systems are dominated by different types of stars.

All three systems are detected by star counts of UMS stars. Although B 164 and Cluster A are found to contain significant samples of LMS stars, they are not revealed at all in the map of the PMS stars (Fig. 6d). On the other hand, the faint stellar populations of the association NGC 602 are certainly PMS and not LMS stars. This demonstrates that both B 164 and Cluster A seem to be evolved small clusters, but NGC 602 is a younger stellar association, with a significant number of PMS stellar members. Consequently, in order to reveal the extent of each system based on its dominant stellar populations we construct their contour maps from star counts of these populations alone, shown in the top panels of Fig. 6. The map constructed for B 164 and Cluster A from the UMS and LMS stars is shown in Fig. 6c, while the one for NGC 602 (from counts of the UMS and PMS stars) is shown on Fig. 6f. We define the boundaries of each stellar system from the 3σ isopleth in these maps. The size of each system is defined by a rectangle, which contains this isopleth.

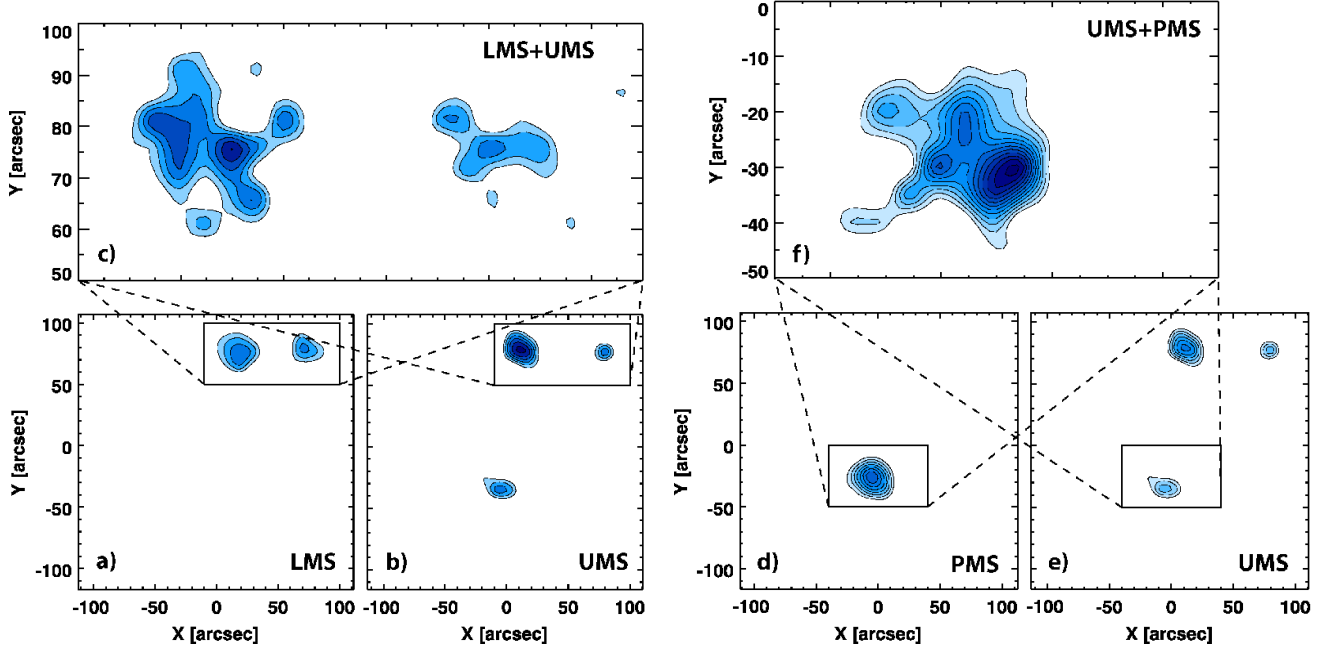


FIG. 6.— Isodensity contour maps for the region of NGC 602/N 90 from star counts of different stellar populations (LMS, UMS, PMS; see §4.1), as they are revealed in the observed CMD. The maps of the whole region (bottom panels) have a grid resolution of $12''$, while the enlarged ones (top panels) of $5''$. In all maps the first drawn density isopleth corresponds to the 3σ significance.

We show in Table 3 the numbers of stars counted within the measured limits of each system (after the field contribution subtracted, see 4.3.1), the surface density and the corresponding fractions of PMS, UMS, and LMS stars included in these limits. These fractions show a clear concentration of PMS stars in NGC 602, while Cluster A and B 164 clearly host the largest amount of LMS stars. Although, both Cluster A and B 164 show to host larger numbers of UMS stars, it is NGC 602 that hosts the brightest MS stars in the region, as it will be shown later from the CMDs of the systems. Considering that the limits for the UMS stars in the CMD have been selected to include stars down to $m_{555} \approx 22.5$ mag, the larger fraction of UMS stars in Cluster A and B 164 is due to their fainter UMS members.

4.3. The Star Clusters B 164 and Cluster A

According to our selection of different stellar types in the observed CMD (§ 4.1), about 55% of the stars in our catalog are LMS stars. Fig. 6a shows that these stars are mostly concentrated in B 164 and Cluster A, but in a rather loose manner (there are only three isopleths above the local background). On the other hand, the concentration of UMS stars in these clusters shows a peak at 9σ above the local background in B 164 (Fig. 6b). The detailed contour map of the area around these clusters, shown in Fig. 6c, shows the prominent concentration of both UMS and LMS stars in both of them (and mostly in B 164) indicating their evolved nature. The absence of PMS stars in both clusters as seen in the map of Fig. 6d, certainly affects their individual CMDs. In order to construct these CMDs we consider the contribution of the stellar population of the general field of SMC in the region, as it is observed within the observed ACS pointing. We apply a Monte Carlo method for the subtraction of this contribution from the CMD observed in the specific area of each cluster.

4.3.1. Subtraction of Contaminating Field Stars

The typical procedure for the field subtraction of a CMD with the use of the Monte Carlo method divides the CMD in a

grid and performs a comparison between the numbers of stars found in each grid element of the observed CMD of the cluster and the one of the region selected as representative of the general field. Although this method is efficient for compact populous star clusters, it might produce unwanted artifacts for smaller not compact clusters or associations. Therefore, our Monte Carlo method for the field subtraction of the observed CMDs of the clusters slightly differs from the typical procedure. Our field-subtraction procedure does not use a predefined grid on the whole extent of the CMDs, but an individual subregion of the CMD is considered around every single star observed in the area of the cluster. Each such subregion has the shape of an ellipse with semi-axes $\Delta(V - I) = 0.15$ mag and $\Delta V = 0.5$ mag.

The corresponding numbers of field and cluster stars inside each of these ellipses (n_F for the field and n_C for the cluster) are counted, and corrected for incompleteness according to the completeness factors estimated per magnitude range for each of the considered areas. The number of field stars per ellipse expected to be present in the CMD of the cluster, n_F^* , is given by the number of field stars, n_F , normalized to the surface of the area of the cluster. The probability that the central star of each ellipse is actually a field star is given by n_F^*/n_C . If e.g. $n_F^* = 0$ then all the stars inside the ellipse are cluster stars and the probability is 0, while if $n_F^*/n_C \geq 1$ then we can assume that this star is actually a field star. For intermediate values, $0 < n_F^*/n_C < 1$, it is randomly decided whether to account this star for a field star or not.

We applied this method to decontaminate the CMD of the area of each system from the contribution of the field. The field-subtracted CMDs of both Cluster A and B 164 are shown in Fig. 7. Their most remarkable feature is the clear MS, which extends from the detection limit up to the brightest stars in the clusters, with magnitudes $m_{555} \approx 16.8$ mag for Cluster A and $m_{555} \approx 15.5$ mag for B 164. An older limit for the age of both clusters can be estimated based on their bright MS stars, with isochrone fitting. We used the models by Girardi et al. (2002), especially designed for the filter system of

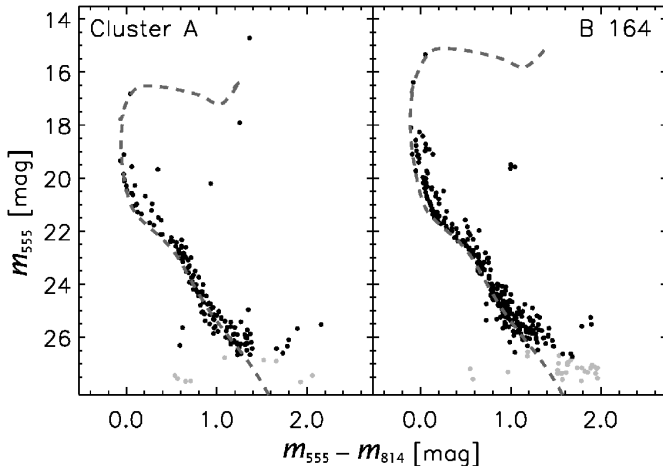


FIG. 7.— The $m_{555} - m_{814}$, m_{555} CMD of the stars in the regions of Cluster A and B 164, after the contribution of the field has been statistically subtracted with the Monte Carlo method. Their prominent MS shows that both clusters are most probably evolved open clusters. The overplotted isochrones from the grid of evolutionary models by Girardi et al. (2002) represent the older limits in the age estimation of each cluster.

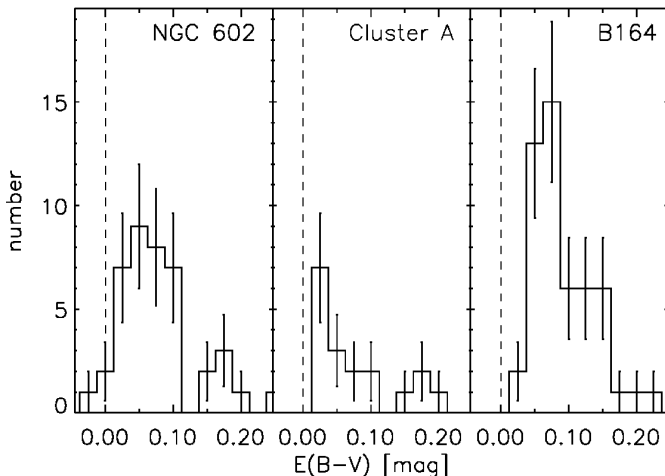


FIG. 8.— The $E(B - V)$ color excess distributions derived from the bright MS stars with $m_{555} < 21.25$ mag in NGC 602 and the clusters B 164 and Cluster A. The peaks of the distributions were estimated assuming that they correspond to a Gaussian distribution. The obtained values are for NGC 602 $E(B - V) = 0.06 \pm 0.02$ mag, for Cluster A $E(B - V) = 0.04 \pm 0.02$ mag, and for B 164 $E(B - V) = 0.07 \pm 0.02$ mag. These values show that all three clusters suffer from rather low optical extinction.

ACS, and we found an age of ≈ 160 Myr for Cluster A, while B 164 is found to be not older than ≈ 80 Myr. It should be noted that if the only bright red star seen in the CMD of Cluster A is also considered, an age of $\tau \sim 80$ Myr may also represent this cluster. If indeed the two clusters have similar ages, and considering that they are very close to each other, one may speculate that both clusters form a double system, product of the same star formation event. However, the available data are not sufficient to support or dismiss this hypothesis.

In Fig. 7 both CMDs are shown with the corresponding isochrones overplotted. In these CMDs, as well as in all CMDs shown here we assume a distance modulus $\mu_0 \simeq 18.9 \pm 0.1$ mag (Dolphin et al. 2001). The largest observed stellar masses for MS stars in each cluster can be estimated from the evolutionary models considered. These masses are $\sim 4.3 M_{\odot}$ for Cluster A and $\sim 5.7 M_{\odot}$ for B 164.

4.3.2. Interstellar Reddening

For the isochrones plotted in Fig. 7 no specific interstellar reddening was considered. The comparison of the loci of the individual UMS stars to the models allowed us an accurate determination of the reddening within the area of each cluster. The corresponding distributions of the stars in Cluster A and B 164 according to their reddening are shown in Fig. 8 (the distribution for NGC 602 is also shown for comparison; see § 4.4). These plots show that a mean color excess of $E(B - V) = 0.04 \pm 0.02$ mag can be considered for Cluster A and $E(B - V) = 0.07 \pm 0.02$ mag for B 164. These values, as well as the one for NGC 602, are in excellent agreement with previous reddening measurements, which vary between $E(B - V) \simeq 0.03$ and 0.07 mag for clusters located in the Wing of the SMC (Piatti et al. 2007), and between $E(B - V) \simeq 0.05$ and 0.09 mag for southern fields of the galaxy (Noël et al. 2007). They are also in good agreement with previous measurements on SMC intermediate-age clusters (e.g. Alcaino et al. 2003; Hunter et al. 2003; Rochau et al. 2007). The reddening values found for Cluster A and B 164 correspond to an extinction of $A_V \approx 0.1$ mag and $A_V \approx 0.2$ mag respectively assuming an extinction law $A_V = R_V E(B - V)$ with $R_V = 3.1$ (e.g. Koornneef 1983).

4.4. The Stellar Association NGC 602

As mentioned earlier (§ 4.2) NGC 602 does not host significant numbers of LMS stars (Fig. 6a), but rather a large concentration of PMS stars (Fig. 6e). The system is also characterized by a prominent UMS stellar population (Fig. 6d). Fig. 6f shows in more detail the morphology of the system based on the spatial distribution of both UMS and PMS stars. This map shows clear signatures of sub-clustering within the system (as is the case for Cluster A and B 164, shown in Fig. 6c), which is demonstrated by the clumpy behavior of the density in the map. Although, this phenomenon could be due to the selection of a finer grid resolution in the star counts (with a grid element size of $\approx 5''$ instead of $12''$, which was used for the larger maps), from the positions of the UMS stars we verified that they are indeed concentrated in smaller sub-regions within NGC 602, the most prominent being the one located to the south-east (bottom-right) of the map in Fig. 6f. This subgroup has also an over-density of PMS stars located with an offset of $\approx 5''$ in respect to the density peak of the UMS stars. A second important subgroup of UMS stars is located $\approx 10''$ east of the first, and as shown in Fig. 6f it is somewhat elongated.

The CMD of the region of NGC 602 is shown in Fig. 9 in comparison to the CMD of the region of the field. NGC 602 shows a more well populated and brighter UMS than Cluster A and B 164, clearly suggesting its youthfulness. We identified the 10 brightest stars of NGC 602 as early-type with spectral types between O5.5 and B0.5. These “photometric spectral types” are consistent (± 0.5 spectral type) with those previously derived by Hutchings et al. (1991) from optical and UV spectroscopy. Moreover, the most prominent feature in its CMD is the large number of stars in the PMS part, which is completely empty in the CMDs of both Cluster A and B 164 and of the field⁴. For the subtraction of the contribution of

⁴ The selection of the region of the field could not be made without including some PMS stars. The reason is that no control field was observed away from NGC 602 and therefore we selected the most “empty” and remote part of the observed FoV as the best representative of the field. The inclusion of PMS stars in the field may lead to the underestimation of the number of PMS stars in NGC 602. However, as derived from the numbers of Table 3, this cannot affect more than 5% of the total PMS members of NGC 602.

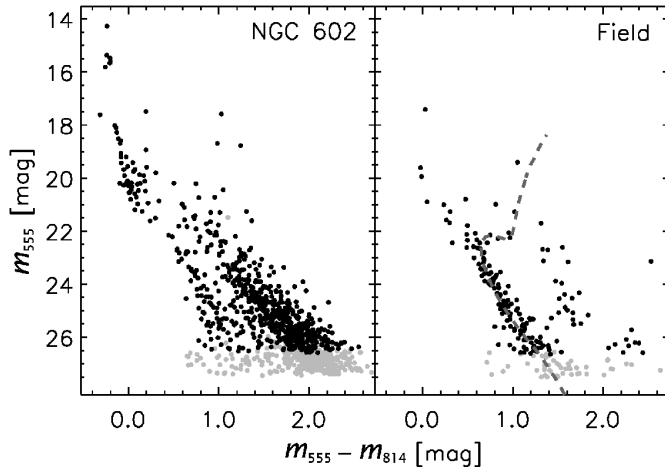


FIG. 9.— The $m_{555} - m_{814}$, m_{555} CMD of the stars in the area of the association NGC 602 (without any subtraction of the contribution of the field), and of the area selected as the most representative of the general background field of the SMC. In the latter, features which are characteristic of the SMC wing stellar population, such as a turnoff at ≈ 22 mag (McCumber et al. 2005), corresponding to the overplotted isochrone of age ~ 1 Gyr, can be distinguished.

the field population in the CMD of NGC 602 we applied the same Monte Carlo method (described in § 4.3.1) as for Cluster A and B 164. The derived “clean” CMD of the stars of NGC 602 alone, shown in Fig. 10, clearly indicates that all the observed LMS stars belong to the field and not the association. The distribution of interstellar reddening for the UMS stars of NGC 602 (Fig. 8) also shows very low extinction. The mean color excess obtained assuming a Gaussian distribution is $E(B - V) = 0.06 \pm 0.02$ mag.

In the CMD of Fig. 10 it can be seen that the positions of the PMS stars show a spread as if they belong to groups of different ages. The observed broadening of the loci of the PMS stars in the CMD implies a wide span in ages of over 10 Myr. Three indicative isochrones of ages 2, 4 and 10 Myr are overplotted in Fig. 10 to demonstrate this spread. If the CMD broadening of the PMS stars is produced by an age-spread or not is very important in understanding the star formation history of the region. The existence of an age-spread would suggest that these stars *did not* originate from a single star formation event, but they were formed over a longer period of time. On the other hand if all PMS stars are the product of a single star formation event, then there should be other factors that affect their CMD positions.

The importance of the age of PMS stars lies on the fact that these stars are the live records of star formation that took place in a star forming region within the last $\lesssim 30$ Myr (e.g. Briceño et al. 2007). Consequently, if we assume that different age-groups of PMS stars can be easily distinguished by their locations in the CMD, they should be the best tracers of any sequential star formation event that might have taken place within their host stellar systems. The age-spread of PMS stars in young stellar systems of our Galaxy has been discussed by e.g. Palla (2005), who notes that the star formation history of the ONC extends long in the past, although at a reduced rate, and by Preibisch & Zinnecker (2007), who found no evidence for an age dispersion in Upper Scorpius OB association, although small age spreads of ≈ 12 Myr cannot be excluded.

However, considering that PMS stars have a rather peculiar behavior, as there are several effects that change their position in the CMD, the retrieval of any signature of age-spread in a

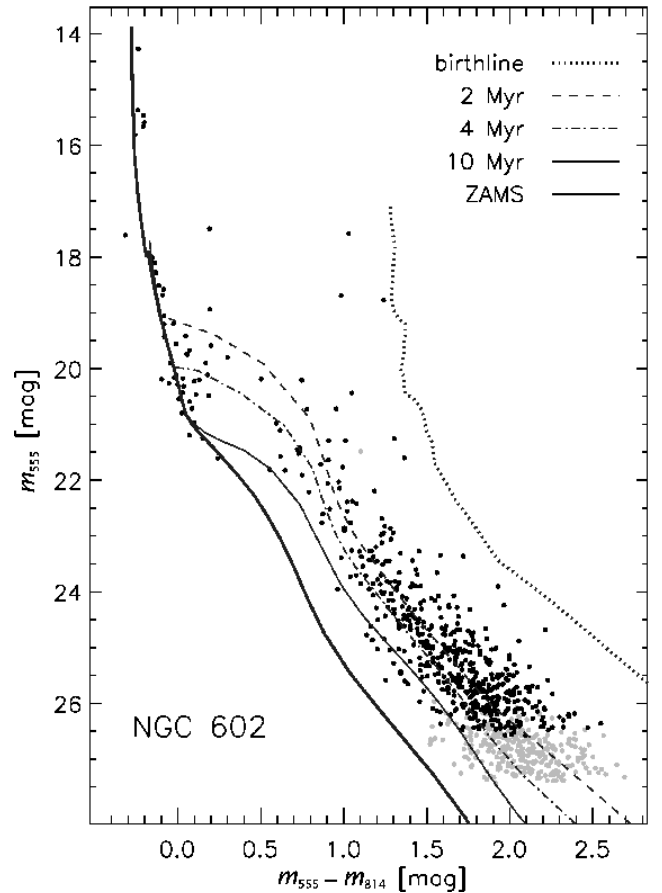


FIG. 10.— The $m_{555} - m_{814}$, m_{555} CMD of the stars in NGC 602, after the contribution of the field has been statistically subtracted with the Monte Carlo method. A clear upper MS (down to $m_{555} \approx 21.5$ mag), as well as a sequence of faint PMS stars (with $m_{555} \gtrsim 21.5$ mag) can be easily distinguished to represent the stellar populations of the association. The loci of the PMS stars show a prominent broadening. This makes the estimation of the age of these stars rather difficult. A discussion on the origins of such a spread in the positions of PMS stars in the CMD is presented in § 4.4. Characteristic isochrones from the grid of PMS models by Siess et al. (2000) are overplotted. The birth-line and the ZAMS from the same grid of models are also plotted.

PMS population with single-epoch photometry alone is not a trivial task. Hennekemper et al. (2008) using the same observational material of another SMC association, NGC 346, showed that there are various physical properties of the PMS stars of the system, which affect their loci in the CMD. This produces a broadening, which could be misinterpreted as an age-spread. These properties, typical for T Tauri stars of our Galaxy, are unresolved binarity, variability and differential extinction. Although it is most certain that these characteristics are responsible for most of the observed CMD broadening of the PMS stars (Hennekemper et al. 2008), one cannot exclude the possibility that there might be also a true age-spread among these stars, hidden in the CMD of NGC 602. We currently explore this possibility in another paper by modeling the observed CMD with the construction of synthetic CMDs for NGC 602 (M. Schmalzl et al., in preparation).

5. LUMINOSITY FUNCTIONS

We constructed the luminosity function (LF) of all three stellar systems by counting the stars in magnitude bins of 0.5 mag in both m_{555} and m_{814} . The m_{555} -LFs of the systems are shown in Fig. 11 for the field subtracted stellar samples shown in Figs. 7 and 10. The LFs of the counted numbers of

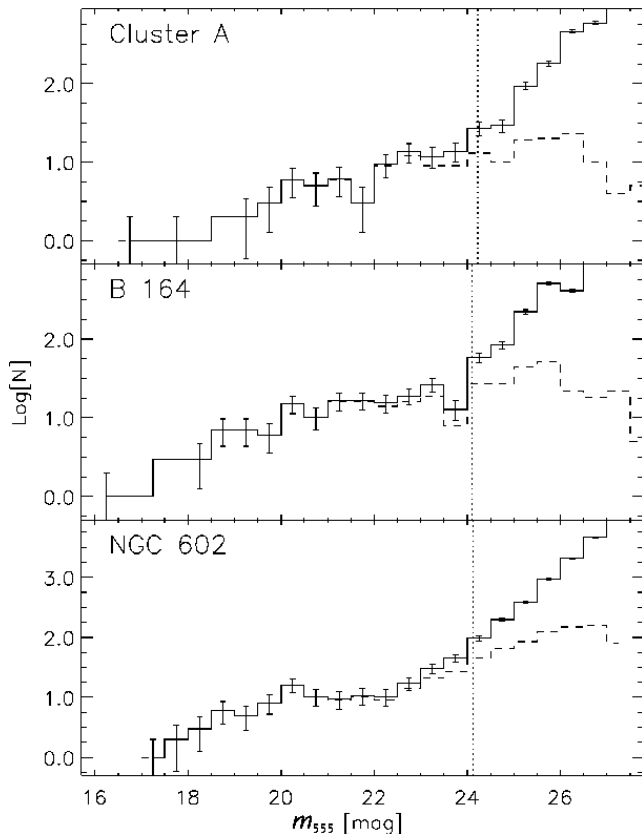


FIG. 11.— The m_{555} -luminosity functions (LFs) for all three stellar systems. The limit of the 50% completeness is indicated in each LF by the dotted lines. The measured numbers of stars are shown with the dashed lines, while the thick lines show the LFs after the stellar numbers have been corrected for incompleteness. In all shown LFs the contribution of field stars has been statistically subtracted.

stars are shown with dashed lines, while the LFs shown with thick lines are corrected for incompleteness. The dotted vertical line for every plot marks the 50% completeness limit for each system. The LFs of both Cluster A and B 164 are very similar, and they both suffer from lower number statistics than the LF of NGC 602 shown in the bottom panel of Fig. 11. In the latter one can identify a small dip at $m_{555} \approx 22$ mag. This feature has been theoretically predicted as a direct consequence of the stellar evolution of young star clusters, since the stars at $m_{555} \approx 21$ mag gain brightness very fast, depleting thus this part of the CMD (Stahler & Fletcher 1991; Fletcher & Stahler 1994).

6. MASS FUNCTION

6.1. Mass Spectrum

The stellar Initial Mass Function (IMF), $\xi(\log M)$, is the distribution of the stars in a stellar system according to their masses, by the time of their formation. The IMF gives the number of stars of the system per unit logarithmic (base 10) mass, $d \log M$, per unit area. There are several functional forms proposed to represent the IMF (see Kroupa 2002 for a review), but its intermediate- and high-mass part (down to $M \approx 1 M_{\odot}$) is generally characterized by a single-power law of the form $\xi(\log M) \sim M^{\Gamma}$. Typical logarithmic derivative is $\Gamma \approx -1.35$, as estimated for stars in the solar neighborhood with masses $0.4 \lesssim M/M_{\odot} \lesssim 10$ (Salpeter 1955). If the stars are counted in unit mass intervals, dM , per unit area, then their Initial Mass Spectrum (IMS), $f(M)$, is constructed. IMS is generally described also by a power law of the form

$f(M) \sim M^{\alpha}$. The IMS and IMF are connected by the relation (Miller & Scalo 1979):

$$f(M) = \xi(\log M) \frac{d \log M}{dM} \quad (1)$$

Consequently, the relation for their indexes (slopes) is:

$$\alpha = \Gamma - 1 \quad (2)$$

For the construction of the IMF or IMS a mass luminosity (ML) relation based on isochrone models is required for the translation of the observed stellar luminosities to masses. However, as shown in § 4.4, the loci of the PMS stars in the CMD of NGC 602 are well spread, producing a broadening which covers a wide range of isochrones (Fig. 10). Since the observed CMD broadening of PMS stars is not solely due to age differences, but also due to the characteristics of these stars (Hennekemper et al. 2008), a construction of a unique ML relation is rather impossible. Specifically, the observed optical magnitudes of young PMS stars are affected by several factors, especially the extinction/emission produced by the accretion disk and/or envelope (e.g. Herbst et al. 2002; Sherry et al. 2004; Briceño et al. 2005). At ages less than 10^7 yr all low-mass PMS stars are variable, and the strength of this photometric variability depends on the star's magnetic activity, the amount of circumstellar matter, and the accretion rate. Classical T Tauri stars are actively accreting gas from circumstellar disks, producing irregular photometric variability with amplitudes up to 3 mag in the V band (Herbst et al. 1994). Naturally, such variations affect the estimation of the luminosities and the effective temperatures for these PMS stars, as well as of their individual circumstellar and differential reddening. Therefore, any attempt to fit isochrone models to the observed CMD and to determine the ages to these stars will be biased⁵.

As a consequence a ML relation cannot be used for the determination of the masses of the observed PMS stars in NGC 602. Therefore, in the following sections we study the IMS of the association, as we constructed it by applying an age-independent approach of counting the PMS stars within PMS evolutionary tracks (e.g. Gouliermis et al. 2006a). For this method we use two different grids of evolutionary tracks, by Palla & Stahler (1999) and Siess et al. (2000), for stellar masses between 0.1 and $6 M_{\odot}$. Both grids cover an age range starting at the birth-line up to ≈ 20 Myr, and they are available in the standard Johnson-Cousins photometric system. In order to compare our CMD to these models we transformed our ACS m_{555} and m_{814} magnitudes to the standard V and I respectively with the use of the transformations provided by Sirianni et al. (2005; § 8.3, and Appendix D). In Fig. 12 we show the transformed $V - I$, V CMD of NGC 602 with the case of counting PMS stars between tracks from the models by Siess et al. (2000). Although the lowest metallicity considered for this grid of models is $Z = 0.01$ (≈ 2.5 times higher than that of the SMC) it fits our data better than the one from Palla & Stahler (1999), which assumes the metallicity of the SMC of $Z = 0.004$. Both grids agree for low mass stars up to $\approx 2.5 M_{\odot}$. For higher masses the models by Palla & Stahler (1999) show a shift to the blue. This can be demonstrated by the comparison of the ZAMS from both grids of models (Fig. 12). The most massive part of the IMS, for stars with $M \gtrsim 6 M_{\odot}$, is occupied by evolved MS stars, and therefore

⁵ See Hennekemper et al. (2008; § 3) for a discussion on the limitations in the age estimation for the PMS stars in the SMC association NGC 346.

another grid of models for such stars, was used. These models were compiled by Girardi et al. (2002) for the standard photometric filter system and the metallicity of the SMC. It should be noted that the ZAMS of Siess et al. (2000) coincides better with the one from Girardi et al. (2002), which match very well the observed MS of the system.

For the construction of the IMS we count all stars with a completeness $\geq 50\%$, and therefore only stars with $m_{555} \lesssim 24.5$ mag, corresponding to $M \gtrsim 1.1 M_{\odot}$ are counted. Considering that each evolutionary track corresponds to a specific mass, we constructed the IMS by counting the PMS stars between evolutionary tracks based on their loci in the CMD. We constructed thus, a histogram with bins defined by the available PMS tracks. It should be noted that building a histogram is the simplest, but by no means optimum, way of analyzing the distribution of masses. Given the uncertainties in our photometry, produced by the characteristics of the PMS stars, which translate into corresponding mass uncertainties, it is possible that some of the objects in every bin might actually have masses slightly outside the bin range. Moreover, Maíz Apellániz & Úbeda (2005) found significant numerical biases in the determination of the slope of power laws from uniformly binned data using linear regression. These biases are caused by the correlation between the number of stars per bin and the assigned weights, and are especially important when the number of stars per bin is small. This result implies the existence of systematic errors in the values of IMFs calculated in this way. As an alternative, those authors proposed to use variable-size bins and divide the stars evenly among them. Such variable-size bins yield very small biases that are only weakly dependent on the number of stars per bin.

Taking into account the above, in order to avoid artificial features in the distribution of the masses, we smoothed our counts by folding them with an adaptive kernel function using a simple boxcar average procedure of 3 mass-bins width. This process smoothes out any random fluctuations due to the fact that some stars could belong to neighboring bins due to the photometric uncertainties and inaccuracies of the evolutionary tracks. Furthermore, in order to properly eliminate any numerical biases in the estimation of the IMS slope due to the bin sizes, the stellar numbers per mass-bin, \tilde{N} , which are used for the IMS, are the counted incompleteness-corrected stellar numbers, N , but normalized to a bin-size of $1 M_{\odot}$, by dividing them to the sizes ΔM of their corresponding bins.

6.2. The Initial Mass Spectrum of NGC 602

The constructed IMS of NGC 602 with the use of evolutionary tracks from both Palla & Stahler (1999) and Siess et al. (2000) is shown in Fig. 13. Small changes in the slope of this IMS, which are apparent in the figure, especially the “knee”-like feature at $\approx 2.5 M_{\odot}$, imply that maybe a multi-power law is appropriate to represent this IMS. However our modeling of the IMS with a weighted linear fit proved that a single-power law of the form $\tilde{N} \sim M^{\alpha}$ describes best this IMS. The slopes derived for the IMS constructed with the use of models by Palla & Stahler (1999) and Siess et al. (2000) show that the use of both grids gives more or less the same results within the derived uncertainties. Specifically, the derived slope for the IMS constructed with the use of the tracks by Palla & Stahler (1999) is found to be $\alpha \simeq -2.0 \pm 0.3$, and the slope derived with the use of the tracks by Siess et al. (2000) $\alpha \simeq -2.4 \pm 0.2$ for the mass range $1 \lesssim M/M_{\odot} \lesssim 45$. It

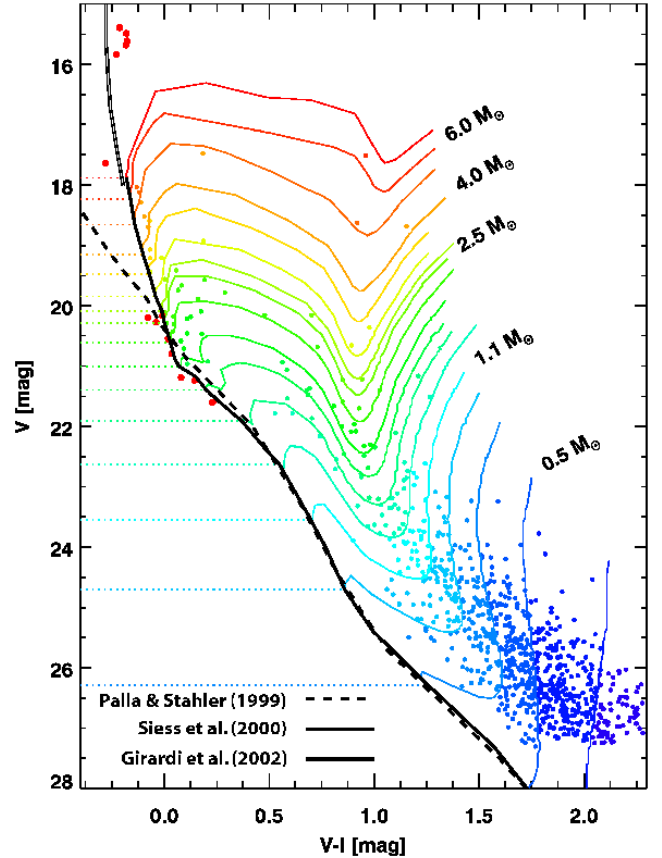


FIG. 12.— Construction of the Initial Mass Spectrum (IMS) of NGC 602 by counting stars between evolutionary tracks. The PMS tracks by Siess et al. (2000) are shown in this plot. The ZAMS of both Siess et al. (2000) and Palla & Stahler (1999) are shown to demonstrate their differences for stars with $V \lesssim 20$ mag. The ZAMS from the grids of models by Girardi et al. (2002), which is found to fit very well the one by Siess et al. (2000) is plotted for the upper MS of the CMD. This ZAMS has been used for the construction of a mass-luminosity relation for the bright MS stars with $M \gtrsim 6 M_{\odot}$ for the derivation of their masses. Different PMS tracks and the stars included between them are plotted in different colors to be easier distinguished.

should be noted that if we compare the derived IMS slopes for specific narrower mass ranges, the largest difference between the used models is seen in the lower mass range of $1 \lesssim M/M_{\odot} < 2.5$ (although these differences are covered by the fitting errors). This is, however, expected from the great differences between the ZAMS of Palla & Stahler (1999) and the one of Siess et al. (2000) shown in Fig. 10, which affects mostly stars with $M \gtrsim 2.5 M_{\odot}$.

Taking into account the results from the application of the linear regression for the IMS constructed with the use of both libraries of evolutionary tracks, the IMS of NGC 602 is best described by the function

$$\tilde{N} \sim M^{-2.2 \pm 0.3} \quad (3)$$

for the whole observed mass range of $\sim 1 M_{\odot}$ up to $\approx 45 M_{\odot}$. The derived mean slope has a remarkable coincidence with the slope of $\alpha = -2.35$ found by Salpeter (1955) for the solar neighborhood, and with the results of Kroupa (2002) who suggests a slope of $\alpha = -2.3 \pm 0.3$ for the mass range of $0.5 \lesssim M/M_{\odot} \lesssim 100$ as the average field star IMF. The IMS of Kroupa (2002) is represented by the shaded region overplotted at the top panel of Fig. 13.

A third IMS to be considered for comparing the IMS of NGC 602 is by Scalo (1998) with a slope of $\alpha = -2.7 \pm 0.5$ for $1 \lesssim M/M_{\odot} \lesssim 10$ and $\alpha = -2.3 \pm 0.5$ for

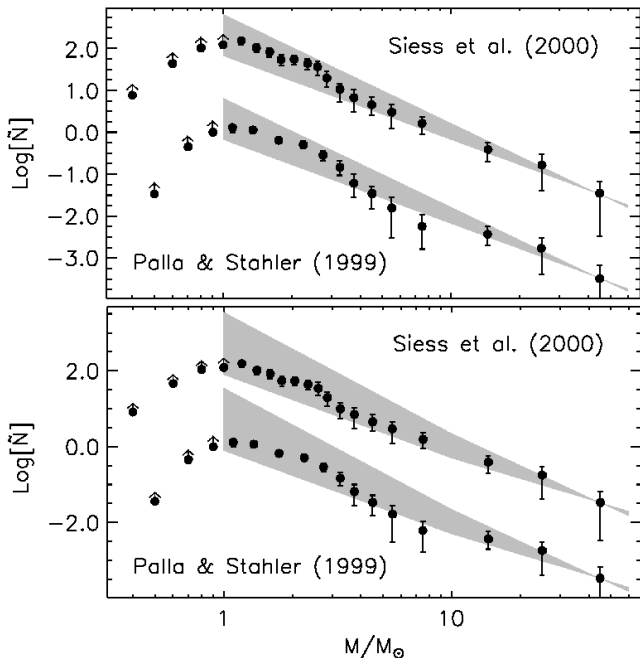


FIG. 13.— The Initial Mass Spectrum (IMS) of NGC 602 as constructed by counting PMS stars between evolutionary tracks and with the use of a ML relation from the models by Girardi et al. (2002) for the brightest MS stars. The derived IMS is shown in each panel from counting PMS stars between tracks from both the models of Siess et al. (2000) (top IMS) and Palla & Stahler (1999) (bottom IMS). The shades at the top panel correspond to a Kroupa (2002) IMS with $\alpha = -2.7 \pm 0.3$, while the ones at the bottom panel to a Scalo (1998) one with $-2.7 \lesssim \alpha \lesssim -2.3$. Stellar numbers \tilde{N} are corrected to a bin-size of $1 M_{\odot}$. A slope of $\alpha \simeq -2.2 \pm 0.3$ is found to represent very well the IMS as it is constructed with the use of all considered grids of models.

$10 \lesssim M/M_{\odot} \lesssim 100$. The slopes we find for the IMS of NGC 602 are comparable also with this IMS for $M \gtrsim 10 M_{\odot}$. For smaller masses the slopes are more different, but still consistent within the errors. The IMS of Scalo (1998) is represented by the shaded region overplotted at the bottom panel of Fig. 13. It is worth noting that our single-power law slope for the IMS of NGC 602 agrees very well with the one found by Gouliermis et al. (2006a) for the stellar association LH 52 in the Large Magellanic Cloud, $\alpha = -2.3 \pm 1.0$. These authors could estimate the IMS slope only for a narrow mass range ($0.8 \lesssim M/M_{\odot} \lesssim 1.4$) due to observational limitations. A multi-power law was found by Preibisch et al. (2002) for the IMS of the whole Upper Sco OB association with the use of data from 2dF, *ROSAT*, and *Hipparcos*. These authors found a slope of $\alpha = -2.8 \pm 0.5$ for $0.6 \lesssim M/M_{\odot} \lesssim 2$ and $\alpha = -2.6 \pm 0.5$ for $2 \lesssim M/M_{\odot} \lesssim 20$. Both these slopes are systematically steeper than the one we found for NGC 602.

6.3. Mass Spectra of Cluster A and B 164

As it is seen earlier from their CMDs, both B 164 and Cluster A are open clusters without any significant PMS population. Therefore, the construction of their mass spectra is more straightforward, since it can be done with the use of mass-luminosity (ML) relations. These relations can be derived from certain models for evolved MS stars (Girardi et al. 2002), and they provide an accurate transformation of luminosities into masses for the stars of these clusters. Naturally, the choice of the appropriate isochrones, as the most representative for the age of the systems, is crucial for this procedure. For this selection we used the upper age limits found earlier (§ 4.3) to be ≈ 160 Myr for Cluster A and ≈ 80 Myr for

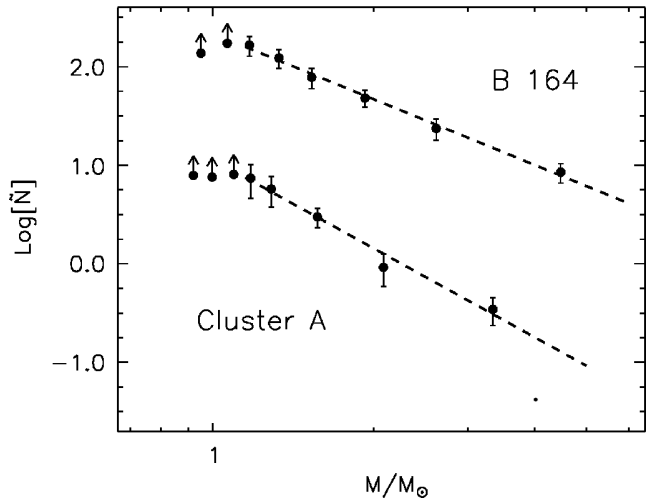


FIG. 14.— The mass spectrum of both B 164 and Cluster A, constructed using ML-relations based on the evolutionary models by Girardi et al. (2002). Points derived from incomplete data (with completeness $< 50\%$) are shown with arrows. The mass spectrum of both clusters is well represented by a single-power law comparable to a Salpeter IMS.

B 164. After obtaining the masses of the cluster members we constructed the corresponding IMS of each cluster, based on the results of Maíz Apellániz & Úbeda (2005), by counting the stars into variable-size mass-bins.

A single-power law is also found to represent the IMS of both clusters for the whole observed mass range with $M \gtrsim 1.5 M_{\odot}$. The best-fitting slopes of the corresponding IMS are found to be:

$$\tilde{N} \sim M^{-2.2 \pm 0.2} \text{ for B 164, } \tilde{N} \sim M^{-2.9 \pm 0.5} \text{ for Cluster A} \quad (4)$$

The IMS slope of Cluster A is found significantly steeper than that of B 164. Specifically, it is interesting to note that the IMS of B 164 is more similar to the one by Kroupa (2002) ($\alpha = -2.3 \pm 0.5$), whereas the IMS of Cluster A fits better to the one by Preibisch et al. (2002) (between $\alpha = -2.8$ and -2.6 ± 0.5) or by Scalo (1998) ($\alpha = -2.7 \pm 0.5$).

7. CONCLUSIONS

We present our photometric study from data obtained in the filters *F555W* and *F814W* with HST/ACS in wide-field mode of the star forming region NGC 602/N 90 in the wing of the SMC. Our aim is to take advantage of the high-resolution efficiency of ACS for the construction of the IMF of the association NGC 602 for the whole observed stellar population of the system. We use the ACS module of the photometric package DOLPHOT, which is especially designed for imaging with the ACS and we provide the full photometric catalog of all stars detected with short and long exposures in one ACS/WFC field that covers a region of about $3'4 \times 3'4$ centered on the young stellar association NGC 602. The region is found to host a mixture of stellar populations. Star counts revealed that there are three prominent stellar concentrations in the observed field: The association NGC 602 itself at the center, and two young open clusters, B 164 (Bruck 1976), and one currently un-cataloged, which we name ‘‘Cluster A’’, both located at the northern edge of the observed area. The CMDs of all three systems are contaminated by the stellar population of the general field of SMC in the region. We selected the most empty (and less contaminated from dust emission, as seen with *Spitzer*; Gouliermis et al. 2007) part of the observed area as the most representative of the general SMC

field. We, then, applied a Monte Carlo method for decontaminating the CMDs of all three identified stellar systems from the contribution of the field.

The CMDs of B 164 and Cluster A show features typical for young open clusters, with a fully populated main sequence extending from the bright part (with only a couple of bright stars in each cluster) down to the detection limit of $m_{555} \sim 28$ mag. By comparing the brightest MS stars of both B 164 and Cluster A we were able to confine their maximum age to be around 80 Myr and 160 Myr respectively. If we consider one red super-giant in the CMD of Cluster A as cluster member, then both clusters have the same age and their close separation suggests that they were possibly formed during the same star formation event. On the other hand, NGC 602 is a much younger system with some bright nebulosity still in its vicinity. The CMD of the association reveals that the stellar members of NGC 602 belong to a rich upper bright main sequence⁶ down to $m_{555} \sim 21$ mag and to a prominent red sequence of faint pre-main sequence stars down to the detection limit. In general, the observed sequence of PMS stars corresponds to an age of roughly 4 Myr. However, there is also a significant amount of PMS stars that can be fitted by a ~ 10 Myr model. The “field”, the area selected as the most representative of the general SMC field, is characterized by a well populated low main sequence and a rather poor red giant branch with a turnoff at $m_{555} \sim 22$ mag. Few stars brighter than the turnoff, and few PMS stars were also included in this area, since it is located within the observed FoV.

We constructed the luminosity functions of all three stellar systems, by counting the stars in magnitude bins of 0.5 mag in both m_{555} and m_{814} . Concerning the mass spectrum of the association, the PMS stars in the CMD of NGC 602 show a prominent broadening, which does not allow a direct measurement of the masses of these stars through a single ML-relation. This broadening might be the result of an age spread, but it could also be due to the characteristics of the PMS stars, such as variability and extinction. In any case the accurate measurement of their age and the estimation of their masses becomes a rather difficult task. Therefore, we constructed the initial mass spectrum of the association with an age-independent method based on counting the PMS stars between evolutionary tracks. We used the grids of models by both Palla & Stahler (1999) and Siess et al. (2000). For the

⁶ The 10 brightest stars in the system are identified as early-type with spectral types between O5.5 and B0.5

bright main sequence stars we used a ML-relation obtained from the evolutionary models by Girardi et al. (2002). The IMS of the association is found to be well represented by a single-power law, corresponding to an IMF of slope $\Gamma \approx -1.2$ for $1 \lesssim M/M_{\odot} \lesssim 45$, similar to the field IMF in the solar neighborhood (Salpeter 1955; Kroupa 2002). No significant differences are found between the IMF derived with the use of Palla & Stahler (1999) models and the one from the models by Siess et al. (2000), although these grids of models are found to be quite different from each other for stars with $m_{555} \lesssim 20$ mag. We also constructed the mass spectra of the clusters B 164 and Cluster A, and we found that the mass spectrum of B 164 corresponds to a mass function similar to NGC 602 with $\Gamma \approx -1.2$, while the one of Cluster A is found to be steeper with $\Gamma \approx -1.9$.

The study of NGC 602/N 90 with observations from *Spitzer*/IRAC by Gouliermis et al. (2007) showed evidence of ongoing star formation on the rim of the H II region. Candidate YSOs were identified by these authors, located around the region of NGC 602, and their formation is most likely triggered through a sequential event initiated at the central association. This hypothesis is currently under investigation within our study of the recent star formation history of this region through the reconstruction of the observed sequence of PMS stars in and around the association in synthetic CMDs (M. Schmalzl et al., in preparation).

D. A. Gouliermis kindly acknowledges the support of the German Research Foundation (Deutsche Forschungsgemeinschaft - DFG) through the grant GO 1659/1-1. We would like to thank the unknown referee for her/his constructive suggestions that helped to improve the manuscript significantly. This paper is based on observations made with the NASA/ESA *Hubble Space Telescope*, obtained from the data archive at the Space Telescope Science Institute. STScI is operated by the Association of Universities for Research in Astronomy, Inc. under NASA contract NAS 5-26555. This research has made use of NASA’s Astrophysics Data System, Aladin (Bonnarel et al. 2000) and the SIMBAD database, operated at CDS, Strasbourg, France.

Facilities: HST(ACS).

REFERENCES

- Alcaino, G., Alvarado, F., Borissova, J., & Kurtev, R. 2003, *A&A*, 400, 917
 Bonnarel, F., et al. 2000, *A&AS*, 143, 33
 Brandner W., Grebel, E. K., Barbá, R. H., et al. 2001, *AJ*, 122, 858
 Briceño, C., Calvet, N., Hernández, J., Vivas, A. K., Hartmann, L., Downes, J. J., & Berlind, P. 2005, *AJ*, 129, 907
 Briceño, C., Preibisch, T., Sherry, W. H., Mamajek, E. A., Mathieu, R. D., Walter, F. M., & Zinnecker, H. 2007, *Protostars and Planets V*, 345
 Bruck, M. T. 1976, *Occasional Reports of the Royal Observatory Edinburgh*, 1, 1
 Davies, R. D., Elliott, K. H., Meaburn, J. 1976, *MmRAS*, 81, 89
 Dolphin, A. E. 2000, *PASP*, 112, 1383
 Dolphin, A. E., et al. 2001, *ApJ*, 562, 303
 Fletcher, A. B., & Stahler, S. W. 1994, *ApJ*, 435, 329
 Girardi, L., et al. 2002, *A&A*, 391, 195
 Gouliermis, D., Brandner, W., & Henning, T. 2005, *ApJ*, 623, 846
 Gouliermis, D., Brandner, W., & Henning, T. 2006a, *ApJ*, 636, L133
 Gouliermis, D. A., Dolphin, A. E., Brandner, W., & Henning, T. 2006b, *ApJS*, 166, 549
 Gouliermis, D. A., Quanz, S. P., Henning, T. 2007, *ApJ*, 665, 306
 Henize, K. G. 1956, *ApJS*, 2, 315
 Hennekemper, E., Gouliermis, D. A., Henning, T., Brandner, W., Dolphin, A. E. 2008, *ApJ*, 672, 914
 Herbst, W., Herbst, D. K., Grossman, E. J., & Weinstein, D. 1994, *AJ*, 108, 1906
 Herbst, W., et al. 2002, *A&A*, 396, 513
 Hester, J. J., et al. 1996, *AJ*, 111, 2349
 Hutchings, J. B., Cartledge, S., Pazder, J., & Thompson, I. B. 1991, *AJ*, 101, 933
 Hunter, D. A., Elmegreen, B. G., Dupuy, T. J., & Mortonson, M. 2003, *AJ*, 126, 1836
 Koekemoer, A. M., Fruchter, A. S., Hook, R. N., Hack, W. 2002, *The 2002 HST Calibration Workshop : Hubble after the Installation of the ACS and the NICMOS Cooling System*, Proceedings of a Workshop held at the Space Telescope Science Institute, Baltimore, Maryland, October 17 and 18, 2002. Edited by Santiago Arribas, Anton Koekemoer, and Brad Whitmore. Baltimore, MD: Space Telescope Science Institute, p.337
 Koornneef, J. 1983, *A&A*, 128, 84
 Kontizas, E., Kontizas, M., Gouliermis, D., Dapergolas, A., Korakitis, R., Morgan, D. H. 1999, *IAU Symposium 190, New Views of the Magellanic Clouds*, eds. Y.-H. Chu et al., 410

- Kroupa, P. 2002, *Science*, 295, 82
- Luck, R. E., Moffett, T. J., Barnes, III, T. G., Gieren, W. P. 1998, *AJ*, 115, 605
- Maíz Apellániz, J., & Úbeda, L. 2005, *ApJ*, 629, 873
- Massey, P. 2006, *The Local Group as an Astrophysical Laboratory*, 164
- McCumber, M. P., Garnett, D. R., Dufour, R. J. 2005, *AJ*, 130, 1083
- Miller, G. E., & Scalo, J. M. 1979, *ApJS*, 41, 513
- Noël, N. E. D., Gallart, C., Costa, E., & Méndez, R. A. 2007, *AJ*, 133, 2037
- Nota, A., et al. 2006, *ApJ*, 640, L29
- Palla, F. 2005, *Massive Star Birth: A Crossroads of Astrophysics*, 227, 196
- Palla, F., & Stahler, S. W. 1999, *ApJ*, 525, 772
- Panagia, N., Romaniello, M., Scuderi, S., & Kirshner, R. P. 2000, *ApJ*, 539, 197
- Piatti, A. E., Sarajedini, A., Geisler, D., Gallart, C., & Wischnjewsky, M. 2007, *MNRAS*, 382, 1203
- Preibisch, T., Brown, A. G. A., Bridges, T., Guenther, E., & Zinnecker, H. 2002, *AJ*, 124, 404
- Rochau, B., Gouliermis, D. A., Brandner, W., Dolphin, A. E., & Henning, T. 2007, *ApJ*, 664, 322
- Romaniello, M., Scuderi, S., Panagia, N., et al. 2006, *A&A*, 446, 955
- Sabbi, E., et al. 2007, *AJ*, 133, 44 (Erratum: 2007, *AJ*, 133, 2430)
- Salpeter, E. E. 1955, *ApJ*, 121, 161
- Scalo, J. 1998, *The Stellar Initial Mass Function (38th Herstmonceux Conference)*, 142, 201
- Sherry, W. H., Walter, F. M., & Wolk, S. J. 2004, *AJ*, 128, 2316
- Siess, L., Dufour, E., Forestini, M. 2000, *A&A*, 358, 593
- Sirianni, M., Nota, A., Leitherer, C., De Marchi, G., & Clampin, M. 2000, *ApJ*, 533, 203
- Sirianni, M., Nota, A., De Marchi, G., Leitherer, C., & Clampin, M. 2002, *ApJ*, 579, 275
- Sirianni, M., et al. 2005, *PASP*, 117, 1049
- Stahler, S. W., & Fletcher, A. B. 1991, *Memorie della Societa Astronomica Italiana*, 62, 767
- Stanimirovic, S., Staveley-Smith, L., van der Hulst, J. M., Bontekoe, T. R., Kester, D. J. M., Jones, P. A. 2000, *MNRAS*, 315, 791
- Venn, K. A. 1999, *ApJ*, 518, 405
- Westerlund, B. E. 1964, *MNRAS*, 127, 429
- Zinnecker, H. 1998, *Highlights in Astronomy*, 11, 136